Quantitative monitoring of radiation induced skin toxicities in nude mice using optical biomarkers measured from diffuse optical reflectance spectroscopy

Darren Yohan,[1,5] Anthony Kim,[3,5,] Elina Korpela,[2] Stanley Liu,[2,4] Carolyn Niu,[2] Brian C Wilson,[2] and Lee CL Chin[1,3,4,*]

[1]Department of Physics, Ryerson University, Ontario, Canada
[2]Department of Medical Biophysics, University of Toronto and Ontario Cancer Institute / Campbell Family Institute for Cancer Research Canada
[3]Department of Medical Physics, Odette Cancer Centre, Sunnybrook Health Sciences Centre Canada
[4]Department of Radiation Oncology, University of Toronto, Toronto, ON, Canada
[5]These authors contributed equally to this work
*Lee.Chin@sunnybrook.ca

Abstract: Monitoring the onset of erythema following external beam radiation therapy has the potential to offer a means of managing skin toxicities via biological targeted agents – prior to full progression. However, current skin toxicity scoring systems are subjective and provide at best a qualitative evaluation. Here, we investigate the potential of diffuse optical spectroscopy (DOS) to provide quantitative metrics for scoring skin toxicity. A DOS fiberoptic reflectance probe was used to collect white light spectra at two probing depths using two short fixed source-collector pairs with optical probing depths sensitive to the skin surface. The acquired spectra were fit to a diffusion theory model of light transport in tissue to extract optical biomarkers (hemoglobin concentration, oxygen saturation, scattering power and slope) from superficial skin layers of nude mice, which were subjected to erythema inducing doses of ionizing radiation. A statistically significant increase in oxygenated hemoglobin ($p < 0.0016$) was found in the skin post-irradiation – confirming previous reports. More interesting, we observed for the first time that the spectral scattering parameters, A ($p = 0.026$) and k ($p = 0.011$), were an indicator of erythema at day 6 and could potentially serve as an early detection optical biomarker of skin toxicity. Our data suggests that reflectance DOS may be employed to provide quantitative assessment of skin toxicities following curative doses of external beam radiation.

References and links

1. E. J. Hall and A. J. Giaccia, *Radiobiology for the Radiologist* (J.B. Lippincott Company, Philadelphia, 2011)
2. J. L. Ryan, "Ionizing Radiation: The Good, the Bad, and the Ugly," J. Invest. Dermatol. **132**(3), 985–993 (2012).
3. J. O. Archambeau, R. Pezner, and T. Wasserman, "Pathophysiology of irradiated skin and breast," In. J. Rad. Oncology Biol. Phys. **31**(5), 1171–1185 (1995).
4. D. Porock, L. Kristjanson, S. Nikoletti, F. Cameron, and P. Pedler, "Predicting the severity of radiation skin reactions in women with breast cancer," Oncol. Nurs. Forum **25**(6), 1019–1029 (1998).
5. R. Noble-Adams, "Radiation-induced skin reactions. 2: development of a measurement tool," Br. J. Nurs. **8**(18), 1208–1211 (1999).
6. C. Westbury, F. Hines, E. Hawkes, S. Ashley, and M. Brada, "Advice on hair and scalp care during cranial radiotherapy: a prospective randomized trial," Radiother. Oncol. **54**(2), 109–116 (2000).
7. A. Yodh and B. Chance, "Spectroscopy and imaging with diffusing light," Phys. Today **48**(3), 34 (1995).

8. A. Amelink, A. P. van den Heuvel, W. J. de Wolf, D. J. Robinson, and H. J. Sterenborg, "Monitoring PDT by means of superficial reflectance spectroscopy," J. Photochem. Photobiol. B **79**(3), 243–251 (2005).
9. Dj. Evers, B. Hendriks, G. Lucassen, and T. Ruers, "Optical spectroscopy: current advances and future applications in cancer diagnostics and therapy," Future Oncol. **8**(3), 307–320 (2012).
10. S. Balter, J. W. Hopewell, D. L. Miller, L. K. Wagner, and M. J. Zelefsky, "Fluoroscopically guided interventional procedures: a review of radiation effects on patients' skin and hair," Radiology **254**(2), 326–341 (2010).
11. N. Kollias, R. Gillies, J. A. Muccini, R. K. Uyeyama, S. B. Phillips, and L. A. Drake, "A single parameter, oxygenated hemoglobin, can be used to quantify experimental irritant-induced inflammation," J. Invest. Dermatol. **104**(3), 421–424 (1995).
12. S. Smesny, S. Riemann, S. Riehemann, M. E. Bellemann, and H. Sauer, "[Quantitative measurement of induced skin reddening using optical reflection spectroscopy--methodology and clinical application]," Biomed. Tech. (Berl.) **46**(10), 280–286 (2001).
13. P. Simonen, C. Hamilton, S. Ferguson, P. Ostwald, M. O'Brien, P. O'Brien, M. Back, and J. Denham, "Do inflammatory processes contribute to radiation-induced erythema observed in the skin of humans?" Radiother. Oncol. **46**(1), 73–82 (1998).
14. M. S. Chin, B. B. Freniere, Y. C. Lo, J. H. Saleeby, S. P. Baker, H. M. Strom, R. A. Ignotz, J. F. Lalikos, and T. J. Fitzgerald, "Hyperspectral imaging for early detection of oxygenation and perfusion changes in irradiated skin," J. Biomed. Opt. **17**(2), 026010 (2012).
15. M. Woo and R. Nordal, "Commissioning and evaluation of a new commercial small rodent x-ray irradiator," Biomed. Imaging Interv. J. **2**(1), e10 (2006).
16. V. Holler, V. Buard, M. H. Gaugler, O. Guipaud, C. Baudelin, A. Sache, M. R. Perez, C. Squiban, R. Tamarat, F. Milliat, and M. Benderitter, "Pravastatin limits radiation-induced vascular dysfunction in the skin," J. Invest. Dermatol. **129**(5), 1280–1291 (2009).
17. L. Chin, W. M. Whelan, and I. A. Vitkin, "Optical Fiber Sensors for Biomedical Applications," in *Optical-Thermal Response of Laser-Irradiated Tissue,* A. J. Welch and M. J. C. van Gemert, eds. (Springer SBM, 2011), pp. 661.
18. A. Kim, M. Roy, F. Dadani, and B. C. Wilson, "A fiberoptic reflectance probe with multiple source-collector separations to increase the dynamic range of derived tissue optical absorption and scattering coefficients," Opt. Express **18**(6), 5580–5594 (2010).
19. A. Kim, M. Khurana, Y. Moriyama, and B. C. Wilson, "Quantification of in vivo fluorescence decoupled from the effects of tissue optical properties using fiber-optic spectroscopy measurements," J. Biomed. Opt. **15**(6), 067006 (2010).
20. P. A. Valdés, A. Kim, M. Brantsch, C. Niu, Z. B. Moses, T. D. Tosteson, B. C. Wilson, K. D. Paulsen, D. W. Roberts, and B. T. Harris, "δ-aminolevulinic acid-induced protoporphyrin IX concentration correlates with histopathologic markers of malignancy in human gliomas: the need for quantitative fluorescence-guided resection to identify regions of increasing malignancy," Neuro-oncol. **13**(8), 846–856 (2011).
21. K. Bekelis, P. A. Valdés, K. Erkmen, F. Leblond, A. Kim, B. C. Wilson, B. T. Harris, K. D. Paulsen, and D. W. Roberts, "Quantitative and qualitative 5-aminolevulinic acid-induced protoporphyrin IX fluorescence in skull base meningiomas," Neurosurg. Focus **30**(5), E8 (2011).
22. J. C. Finlay and T. H. Foster, "Hemoglobin oxygen saturations in phantoms and in vivo from measurements of steady-state diffuse reflectance at a single, short source-detector separation," Med. Phys. **31**(7), 1949–1959 (2004).
23. S. Prahl, "Tabulated Molar Extinction Coefficient for Hemoglobin in Water," *http://omlc.ogi.edu/spectra/hemoglobin/summary.html.*
24. J. R. Mourant, T. Fuselier, J. Boyer, T. M. Johnson, and I. J. Bigio, "Predictions and measurements of scattering and absorption over broad wavelength ranges in tissue phantoms," Appl. Opt. **36**(4), 949–957 (1997).
25. L. Chin, B. Lloyd, W. M. Whelan, and A. Vitkin, "Interstitial point radiance spectroscopy of turbid media," J. Appl. Phys. **105**(10), 102025 (2009).
26. A. Corlu, T. Durduran, R. Choe, M. Schweiger, E. M. Hillman, S. R. Arridge, and A. G. Yodh, "Uniqueness and wavelength optimization in continuous-wave multispectral diffuse optical tomography," Opt. Lett. **28**(23), 2339–2341 (2003).
27. A. Kim and B. C. Wilson, "Measurement of Ex Vivo and In Vivo Tissue Optical Properties," in *Optical-Thermal Response of Laser-Irradiated Tissue,* A. J. Welch and M. J. C. van Gemert, eds. (Springer, 2010), pp. 267.
28. J. D. Rogers, I. R. Capoğlu, and V. Backman, "Nonscalar elastic light scattering from continuous random media in the Born approximation," Opt. Lett. **34**(12), 1891–1893 (2009).
29. V. Turzhitsky, N. N. Mutyal, A. J. Radosevich, and V. Backman, "Multiple scattering model for the penetration depth of low-coherence enhanced backscattering," J. Biomed. Opt. **16**(9), 097006 (2011).
30. K. Vishwanath, D. Klein, K. Chang, T. Schroeder, M. W. Dewhirst, and N. Ramanujam, "Quantitative optical spectroscopy can identify long-term local tumor control in irradiated murine head and neck xenografts," J. Biomed. Opt. **14**(5), 054051 (2009).

1. Introduction

Radiation therapy (RT) in medicine is the application of high doses of ionizing radiation as a means of treating and / or controlling malignant growths. Despite efforts to avoid toxicities to normal tissues, radiation induced skin reactions are a common side effect of treatment resulting in significant distress and discomfort to patients [1]. Such acute effects include erythema and manifestations of moist desquamation and ulceration in more serious cases. In extreme cases, surgical treatment may be required in the case that a wound progresses to a deeper lesion [2]. While damage to the basal skin layer has typically been shown to occur at ~20-25 Gy (~10 fractions) [3], a variety of risk factors exist, which complicate the specific threshold dose and severity of toxicity from patient to patient [4]. These reactions tend to progress throughout treatment and can persist beyond completion of the treatment. However, very little data exists on patient experience of skin reactions, and the management of such toxicities has been anecdotal rather than evidence-based. Hence, a systematic means of monitoring the onset of RT-induced acute skin toxicities prior to full progression may offer a patient-specific means of managing skin reactions and intervention for wound prevention and healing. Current scoring systems for radiation skin reactions (i.e. RISRAS or RTOG scoring) require a qualitative clinical manifestation of the skin toxicity and are often criticized for their subjectivity [5,6].

Diffuse optical spectroscopy (DOS) is a technique that has the potential to provide quantitative assessment of functional changes in tissue including hemoglobin content, oxygen saturation and tissue scattering power [7]. Wide ranging applications of DOS include, but are not limited to, measurement of blood volume and saturation during photodynamic therapy as well as cancer diagnostics [8,9]. Epithelial cell death and stimulation of other cells due to radiation induce a vasodilatory effect that is expected to induce a change in the blood content within the skin microvasculature. As such, the DOS technique is well suited to the expected physiological changes in skin during radiation therapy [10–12]. However, only limited studies exist evaluating the potential of DOS for ongoing treatment monitoring of RT induced skin toxicities – particularly at early time-points following radiation exposure [13,14]. Furthermore, previous reports have employed "black-box" commercial systems that report only on hemoglobin and oxygen saturation parameters, while assuming constant optical path-length (i.e. contact scattering properties) and may provide an incomplete picture of all potential optical biomarkers.

In this paper a diffuse optical spectroscopy fiberoptic probe is utilized to measure real-time hemoglobin, oxygen saturation levels and scattering parameters in skin following erythema inducing levels of external beam radiation (40 Gy) in mice at two superficial probing depths. The method presented here can be used in normal lighting conditions, is portable, safe, clinically translatable and delivers readings in near real-time (1 - 3 seconds). The long term goal of this work would be to design an appropriate DOS probe for translational clinical trials in breast and head and neck cancer patients that could be employed to perform real-time monitoring for early patient specific intervention with anti-inflammatory creams and drugs prior to severe radiation reactions.

2. Methods

2.1. Mice and irradiation

Six-week old female athymic nude mice were employed in this study. These mice are unable to produce functional T cells due to the absence of a thymus and are therefore unable to mount a normal adaptive immune response. Notwithstanding, they exhibit an early innate immune response and inflammation through neutrophil and macrophage recruitment and cytokine signaling. All animals were handled in accordance with protocols approved by Sunnybrook Research Institute's Animal Care Committee. The mice were divided into irradiated (n = 8) and non-irradiated (n = 3) groups. Box-shaped lead shielding was placed

over the mice and loose right side flank skin was pulled through an opening in the shielding. The pulled skin was taped down to the platform to be irradiated. An area no larger than 4 cm^2 on the skin surface was exposed to 40 Gy of ionizing radiation. The Faxitron model CP160 (Faxitron X-Ray Corp., Wheeling, IL) was used to irradiate the animals and was previously commissioned and evaluated at our centre for use with small rodents [15].

Figure 1 shows a sample of the irradiated mice 12 days after receiving the dose showing varying degrees of skin toxicity. Spectra were collected at 3-5 points on each mouse for a total of 208 measurements. Points taken on blistered or scabbed skin were eliminated from the average.

Fig. 1. Photograph of irradiated mice 12 days receiving 40 Gy of 120 kvP x-rays. Varying degrees of skin toxicities (erythema, scabs, scar tissue) were observed.

Median radiation skin damage scores were tabulated on days 0, 6, 9 and 12 following irradiation (Table 1). This qualitative scoring system has been used previously by Holler et al. [16] and is similar to the acute skin toxicity scales used to evaluate the extent of skin damage as a result of cancer radiotherapy. Toxicity scoring ranged from 0 "normal" to 3 "desquamation of most of the irradiated area".

2.2 Fiberoptic Probe

Optical fiber sensors have been employed since the 1960s and provide an affordable and safe method for delivering and collecting light within a tissue volume of interest [17]. The fiberoptic probe employed in this study has been described previously by Kim et al. [18,19] and was originally designed to perform fluorescence and diffuse optical spectroscopic measurements to aid in guiding the resection of glioma during neurosurgery [20–22]. Figure 2 shows a typical operational schematic of the device's key features. The source fiber uses visible white light emitted from a light-emitting diode (LED). Diffuse reflectance spectra were collected at a fixed distance from the source.

The two fixed source-collector distances, 260 μm and 520 μm, were designed for optimal sensitivity for assessing skin response (~1 - 2 mm into the skin respectively). Scan times were rapid, ranging from 1 to 3 seconds.
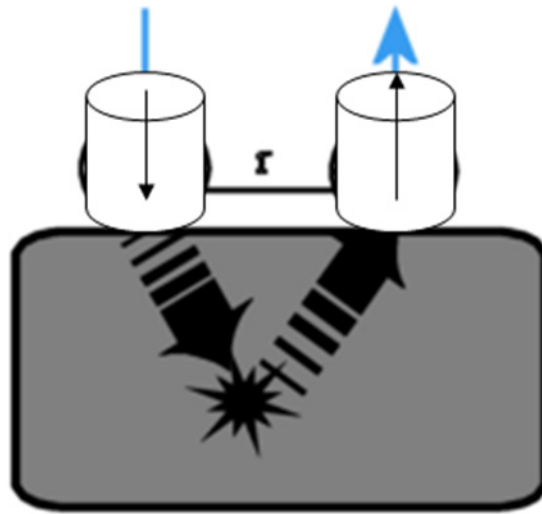
Fig. 2. An operational schematic of the fiberoptic probe employed. Broadband light is used to illuminate the tissue (via an optical fiber) and diffuse reflectance spectra are collected at a fixed distance from the source via a collection fiber.

Figure 3 shows a schematic of the probing depth and relevant skin tissues. The probe was calibrated as per the method used by Kim et al. [18] and included the taking of a reference spectrum to compensate for variations in LED output. As the probe allows for background light subtraction, it can be used in normal lighting conditions [18,19]. Light contact pressure was always used to minimize compression of the local vasculature.
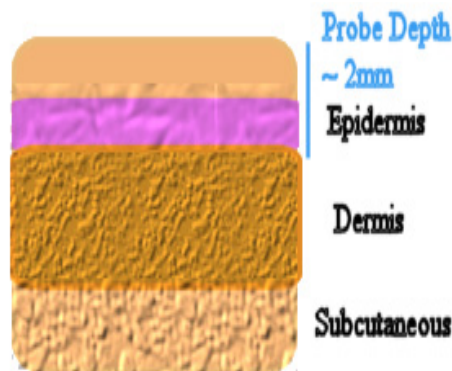

Fig. 3. Optical probing depth relative to relevant skin sections. Source-detector separations were chosen to optimize sensitivity to the epidermal layer (~1-2 mm).

2.3 Spectral analysis

For bulk tissues, the wavelength dependence of the reduced scattering coefficient, $\mu_s'(\lambda)$, can be approximated using a power law dependence for point reflectance fitting [22]:

$$\mu_s'(\lambda) = A\left(\frac{\lambda}{\lambda_o}\right)^{-k} \tag{1}$$

where A (cm^{-1}) is the value of μ_s' at $\lambda_o = 1$ nm and k is a medium dependent power factor. Using $\lambda_o = 1$ nm, Eq. (1) takes the form originally proposed by Mourant et al. [23] who suggested that k may be related to the average scatterer size of the medium and has been shown to be a reasonable description of the scattering spectrum of both biological tissues and tissue-simulating Intralipid phantoms [23,24]. Equation (1) was previously verified by our group for spectral fitting in tissue simulating phantoms for the same DOS probe geometry employed in this study [18].

The particular shape of $\mu_a(\lambda)$ is dependent on the chromophores of the medium of interest and their respective concentrations. Here we perform an analysis using oxy, $\mu_a^{oxyHb}(\lambda)$, and deoxy, $\mu_a^{deoxyHb}(\lambda)$, hemoglobin. The hemoglobin, H_b, basis spectra were obtained from the on-line collection of Prahl [25]. In this case $\mu_a(\lambda)$ takes the form:

$$\mu_a(\lambda) = H_b \left[StO_2 \mu_a^{oxyHb}(\lambda) + (1 - StO_2) \mu_a^{deoxyHb}(\lambda) \right] \qquad (2)$$

where H_b is the total hemoglobin concentration in g/L, and StO_2 is the oxygen saturation ranging from $0 - 1$.

Equation (2) is representative of the absorption spectra in the near-infrared for typical biological tissues, which are dominated by oxy-, deoxy-hemoglobin. Note that water absorption was neglected in this study due to negligible contribution within our spectral analysis range (450-650 nm) while melanin absorption was not included as the measurements were performed on nude albino mice lacking melanin. In practice, both these chromophores could also be implemented in Eq. (2) in human trials with DOS devices spanning a broader wavelength spectrum.

To extract the optical parameters, the measured reflectance spectra were fit to a forward diffusion theory model of light transport, which has been extensively validated for the given probe geometry to accurately recover optical properties spanning those expected in biological tissues [18]. It has been previously demonstrated that spectrally constraining the fit to Eqs. (1) and (2) provides a unique set of oxygen concentration, oxygen saturation and scattering parameters with only constant wave broadband measurements [18,22,25,26].

The inverse fitting was performed using an iterative algorithm that utilized randomly generated test parameters to determine the coefficients that best fit the non-linear diffuse reflectance equation. By setting total H_b, StO_2, A and k used as free coefficients, the parameters were extracted by the iterative algorithm. This algorithm was implemented using MatLab's lsqcurvefit function (Mathworks Inc., Natick, MA). Fits that resulted in a squared 2-norm of the residual sum above a given threshold were discarded but these constituted less than 3% of the total measurements taken. Spectra were processed in the same way as described by Kim et al [18]. Spectra were collected on Days 0, 6, 9, and 12 relative to the time of radiation. The values for each individual mouse on days 6-12 were normalized to each one's unique baseline reading on day 0.

2.4 Statistical analysis

Each mouse was averaged over the 3-5 points measured. A p-value was calculated based on the average for each mouse and comparisons were made for each parameter and each day between both groups at both source-collector separations. P-values were calculated using a one-way analysis of variance. Results were judged to be significant if the p-value was < 0.05 for relative differences between the irradiated group and the control group. P-value calculations, including a Kolmogorov-Smirnov one sample goodness of fit test for normality were done via Matlab's StatisticsToolbox (Mathworks Inc., Natick, MA).

3. Results

The median radiation skin damage scores for each mouse are shown for days 6, 9 and 12 following the 40 Gy skin irradiation in Table 1. Skin damage severity increased until day 12. These values remained at the peak score of ~3 until day 16 (data not shown) and decreased upon wound healing until the time of sacrifice on day 28. The tabulated values were correlated with DOS measurements up to the time of peak skin toxicity (day 12).

Table 1. Qualitative scores [16] for skin reaction for irradiated mouse group.

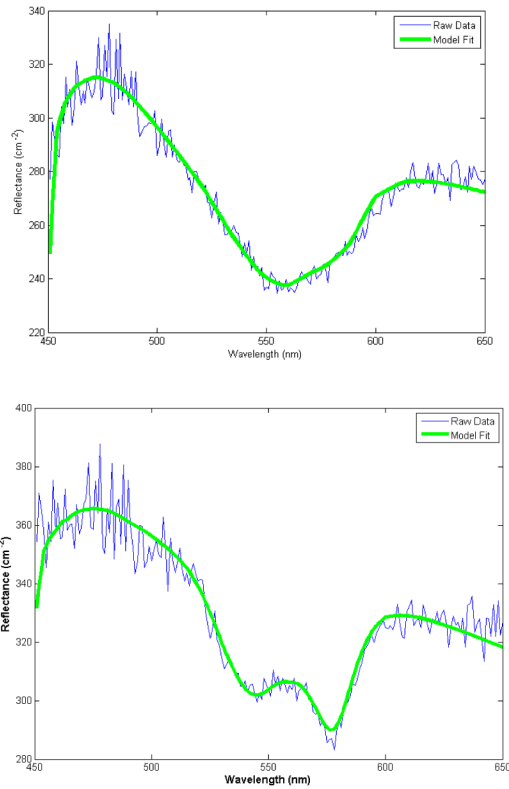| Day	Mouse 1	Mouse 2	Mouse 3	Mouse 4	Mouse 5	Mouse 6	Mouse 7	Mouse 8
0	0	0	0	0	0	0	0	0
6	0.75	0.75	0.75	0.75	0.75	0.75	0.75	0.75
9	1.25	1.25	1.5	1.5	1	1.5	1.75	1.25
12	3.25	2.75	3	2.5	2.25	3	3	3

Fig. 4. Typical white light reflectance spectra of non-irradiated (top) and irradiated (bottom) mouse skin 6 days post irradiation. Thin blue lines are the measured data while solid green lines are the respective fits. Excellent agreement between measurement and fits were typically observed. Two key differences were seen between the two groups: 1) an overall increase in absolute reflectance and 2) a distinct change in spectral shape between 550 – 600 nm.

Figure 4 shows typical measured spectra (thin blue lines) 6 days post irradiation for both the irradiated group and the non-irradiated control group along with the associated fits (thick green lines). Excellent agreement between the measured and fitted data was typically observed, validating the chosen chromophores employed during fitting. Qualitatively, an overall increase in absolute reflectance was typically observed. Such changes are generally associated with either a decrease in absorption (i.e. decreased hemoglobin) or an increase in scattering power. In addition, a distinct change in spectral shape between ~550 – 600 nm was

observed - indicating changes in the oxygen saturation due to irradiation. Similar trends were observed for the 520 μm separation. These key features in the spectra are what allow the extraction of optical parameters via the fitting algorithm and the forward model.
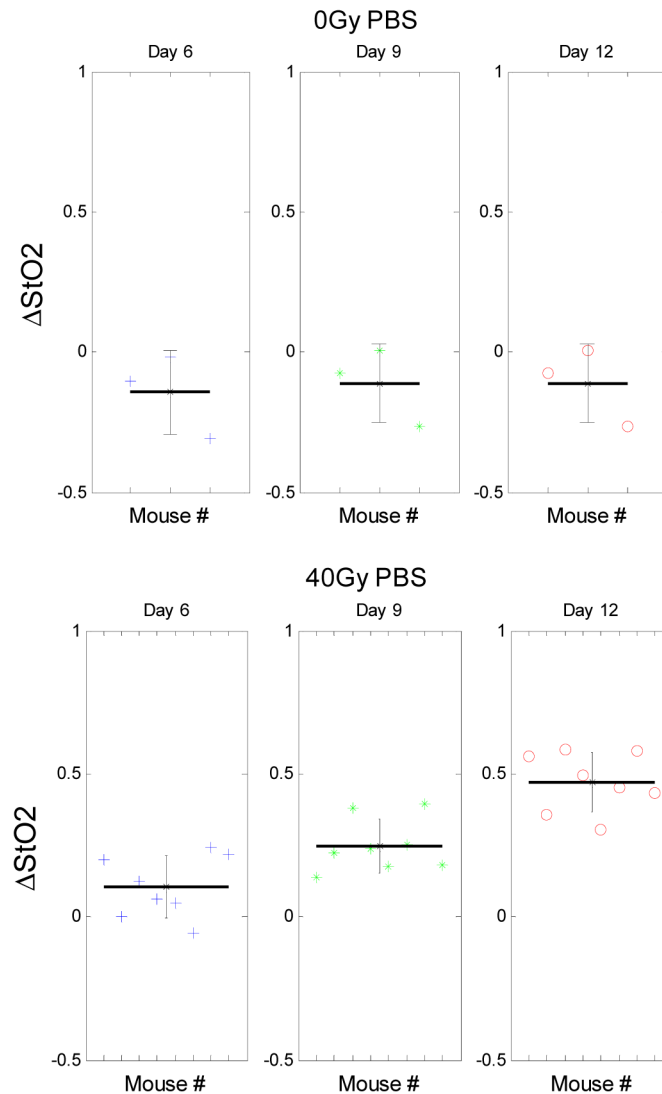

Fig. 5. Change in the oxygenation fraction for the non-irradiated group (top) and irradiated group (bottom). Individual mouse points are shown along with the average (black bar) and error bars depicting standard deviation. The baseline-normalized mean difference between the two groups (per mouse) is significant for Days 6-12 as shown in Table 2.
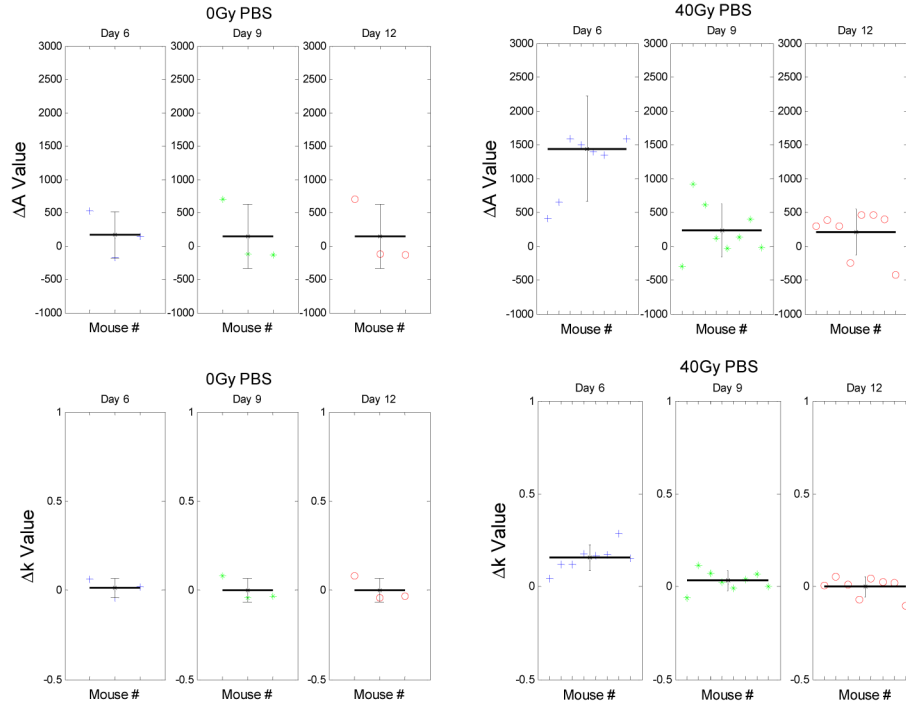
Fig. 6. Top and bottom left show the relative time-resolved changes in A and k for the control group. Top and bottom right depict the same for the irradiated group. The change in A and k on Day 6 was found to be significant (p < 0.026).

Figures 5 and 6 shows the changes in StO$_2$ and A / k, respectively for the entire cohort of mice for days 6, 9 and 12 post irradiation measured at the 260 μm source-detector separation. Similar trends were observed for the 520 μm separation (data not shown visually but summarized in Table 3). A small statistically insignificant decrease in StO$_2$ was observed in the control group that may have been due to an injection of phosphate buffer solution. While all other optical parameters remained near baseline levels for the non-irradiated group, there is a distinct increase in the StO$_2$ parameter over the 12 days in the irradiated group (Fig. 5). Furthermore a significant increase in the parameters A and k on Day 6 was observed for the irradiated group that was not seen in the control group (Fig. 6).

Table 2. Average relative change in hemolobin (ΔHb), oxygenation fraction (ΔStO2), A (ΔA) and k (Δk) for the 260 μm source-collector pair on day 6, 9 and 12 for irradiated mice relative to day 0.

	Day 6	Day 9	Day 12
ΔHb	0.52	0.14	0.64
ΔStO2	0.11*	0.25*	0.47*
ΔA	1438*	232	206
Δk	0.16*	0.032	−0.0015

* indicates significant difference (p < 0.05) between control and radiated group calculated over the average for each mouse

Table 2 summarizes the average relative change (Δ) from Day 0 (pre-irradiation) of the recovered optical parameters from the 260 μm separation reflectance spectra 6, 9 and 12 days post-irradiation for irradiated group, and * denotes the changes that are statistically significant from the non-irradiated control group. Table 3 summarizes similar results for the 520 μm

separation. Statistically different parameters from the control group for each time point are denoted by the asterisk.

Table 3. Average percent relative change in hemolobin, oxygenation fraction, A and k for the 520 μm source-collector pair on day 6, 9 and 12 for irradiated mice relative to day 0.

	Day 6	**Day 9**	**Day 12**
ΔHb	0.47	2.56	0.74
ΔStO2	0.078	0.27*	0.44*
ΔA	152*	−4.9	−44
Δk	0.07*	−0.01	−0.05

* indicates significant difference (p < 0.05) between control and radiated group calculated over the average for each mouse

There were no significant changes in the control group for any of the parameters over the 12 days with optical parameters remaining similar to baseline. In contrast, a statistically significant increase occurs for a variety of DOS parameters between days 6 – 12 mirroring the qualitative increase in skin toxicity in Table 1.

As shown in Table 2 (260 μm separation), significant differences between the control group and the irradiated group occurred on days 6-12 (p = 0.013; 7.2×10^{-4}; 2.8×10^{-5} respectively) for the oxygenation fraction, day 6 *only* for the A value (p = 0.026) and day 6 *only* for the k value (p = 0.011). Table 2 also shows that there was no significant difference in the total hemoglobin between the irradiated group and the control group. The parameter *k* exhibits some fluctuation in the control group largely due to fitting noise. Measurements performed at the 520 μm separation mirrored those at 260 μm with the only difference being a lack of statistical difference compared to the control group for ΔStO2 on Day 6. This is possibility due to a lack of skin specific depth sensitivity at this source-detector distance.

4. Discussion and conclusions

Current methods for scoring skin toxicity are based on qualitative evaluation and are prone to inter-observer subjectivity. Inter observer variability is of concern for skin toxicity evaluation during external beam radiation therapy as non-standardized, anecdotal training between treatment units and inexperience from rotating trainees could result in missed diagnosis. As such, a number of groups have recently explored the potential of quantitative measures that could be translated to automated skin toxicity scoring.

In this study, we have investigated the potential of optical biomarkers measured using a portable, real-time DOS reflectance probe for on-line skin toxicity scoring. A key feature of the described probe was the ability to accurately measure functional optical parameters at superficial depths similar to skin thickness [18]. In the case of mouse skin, a 260 μm source-detector separation was shown to be most sensitive to developing skin toxicity. While similar trends were observed at a 520 μm separation, much smaller relative changes occurred following irradiation indicating a correspondingly decreased sensitive probing depth beyond the skin layer of inflammatory response. We note that this might not be the case for human skin, which could have thicker epidermal layers than mice. As such, the described probe provides a dynamic depth range that is flexible for pre-clinical and translational studies.

In evaluating diffuse optical spectroscopy (DOS) for the purpose of monitoring radiation induced erythema, we have found that DOS was effective in distinguishing the hemoglobin oxygenation fraction between the irradiated group and the control group. These results confirm previous studies that have shown a strong correlation between oxygen saturation and erythema [11,12,14]. Most notably, Chin et al. [14], observed two distinct oxygen saturation response peaks at Day 1 and ~Day 10 following a 50 Gy dose of beta particle irradiation. Although they employed an immune competent mouse model, we observed similar trends in

our athymic model. While our current study did not evaluate optical response at day 1, we observed a similar peak response between days 9-12. The same group observed an increase in total hemoglobin concentration that was also seen as a subtle trend in our study. However, these measured increases were more variable both temporally and as a function of depth and were not shown to be statistically significant in the present study.

A key difference of our work from previous studies is the use of a spectral fitting algorithm and probe design that allows for the separation of *both* absorption and scattering parameters. This is in contrast to non-contact (camera) constant wave hyperspectral imaging techniques that assume a constant optical path-length (i.e. constant scattering) during fitting and, as such, neglect potential changes in *A* and *k*. Such an assumption introduces a potential source of error in the spectral fitting algorithm – particularly if significant scattering changes exist. In addition, both parameters, *A* and *k*, are related to the bulk structural state of the underlying tissue (i.e. average scatterer size and spacing) [24,25,27–29] and could provide additional biometric information for classifying skin toxicity.

Our finding that both *A* and *k* were significantly different on Day 6 for both source-collector separations is noteworthy and is, to our knowledge, the first report of tissue scattering changes due to radiation induced inflammation. In particular, we note that the "scattering spike" on Day 6 coincided approximately with the time of initial visual manifestation of erythema but returned close to baseline values between Days 9 – 12 even while oxygen saturation and visual scoring continued to increase. While the underlying mechanisms are unclear, we speculate that the observed scattering increase could be due to apoptosis and swelling followed by a rapid clearance of cellular debris beyond days 9 – 12. Regardless, a potential implication of this trend is that scattering changes could be an early optical biomarker of inflammatory manifestation prior to full visual manifestation and could be useful for interventional therapy. While absorption-based visual changes (i.e. reddening) are relatively evident, small scattering changes may be difficult to discern and underscores the importance of quantitative toxicity scoring metrics.

To further investigate the detection of the inflammatory response using the above parameters, future studies would benefit from acquiring data at more frequent intervals as well as on days 1 and 2 following radiation exposure when the inflammatory response is just beginning. Furthermore, the inclusion of expanded wavelengths up to ~1000 nm would allow for the fitting model to include the effects of water – an additional optical biomarker. We note that lack of melanin in the athymic mice employed in this work may have allowed for the emergence of the scattering parameters as potential optical biomarkers. Melanin has been previously shown to produce cross-talk with the similarly monotonic shape of spectral scattering and may complicate the sensitivity of *A* and *k* when employed in humans. This potential cross-talk will be addressed in future studies.

The 40 Gy dose and use of immune compromised mice employed in this study was used to accelerate the onset of erythema to complete the experiments within a practical timeline. Clinically, patients undergoing radiation therapy receive daily fractionated doses (~2 Gy/fraction). They exhibit immune responses over several weeks of treatment allowing for interventional therapies to be administered prior to the onset of severe skin reactions. As such, early signs of erythema could conceivably be detected using a weekly monitoring protocol. Current work is underway to ascertain if the DOS system is sensitive enough at early time points (i.e. Days 1-3) to predict erythema and mimic the more gradual evolution of skin toxicity in a clinical setting.

In summary, we have demonstrated the potential of optical biomarkers for scoring and quantifying skin toxicity. Furthermore, we have employed a clinically translatable DOS probe that is patient-friendly owing to its portability, quick response time and ability to be used in normal lighting conditions. We note that since the DOS probe requires gentle contact with skin, clinical translation to patients would incorporate a systematic approach for mediating probe pressure.

Ultimately the clinical use of monitoring such parameters in the irradiated skin of cancer patients would be as predictive biomarkers if early DOS measurements can identify those patients at risk of developing severe radiation skin toxicity. Conceivably, patients who show signs of developing severe radiation skin toxicity could be administered an interventional therapy to minimize the outcome (e.g. biological targeted agent). Such therapies are of importance for improving cosmetic outcome and, more importantly, for maintaining patient compliance in completing radiation treatment over a protracted 6 – 8 week fractionated course. In addition, an exciting possibility is to use the same DOS probe to concurrently assess treatment response to radiation therapy at the tumor site [30].

Acknowledgments